# Open Research Online

The Open University's repository of research publications
and other research outputs

## Potential effects of atmospheric collapse on Martian heat flow and application to the InSight measurements

### Journal Item

## oro.open.ac.uk

# Potential effects of atmospheric collapse on Martian heat flow and application to the InSight measurements

N. Attree [a,*], N. Patel [b], A. Hagermann [a,b], M. Grott [c], T. Spohn [c], M. Siegler [d]

[a] Earth and Planetary Observation Centre, Natural Sciences, University of Stirling, UK
[b] School of Physical Sciences, The Open University, Milton Keynes, UK
[c] DLR Institute for Planetary Research, Berlin, Germany
[d] Deadman College of Humanities and Sciences, Southern Methodist University, Dallas, USA

A B S T R A C T

Heat flow is an important constraint on planetary formation and evolution. It has been suggested that Martian obliquity cycles might cause periodic collapses in atmospheric pressure, leading to corresponding decreases in regolith thermal conductivity (which is controlled by gas in the pore spaces). Geothermal heat would then build up in the subsurface, potentially affecting present–day heat flow — and thus the measurements made by a heat–flow probe such as the InSight $HP^3$ instrument. To gauge the order of magnitude of this effect, we model the diffusion of a putative heat pulse caused by thermal conductivity changes with a simple numerical scheme and compare it to the heat–flow perturbations caused by other effects. We find that an atmospheric collapse to 300 Pa in the last 40 kyr would lead to a present–day heat flow that is up to $2 - 8\%$ larger than the average geothermal background. Considering the InSight mission with expected $5 - 15\%$ error bars on the $HP^3$ measurement, this perturbation would only be significant in the best-case scenario of full instrument deployment, completed measurement campaign, and a well–modelled surface configuration. The prospects for detecting long-term climate perturbations via spacecraft heat–flow experiments remain challenging.

## 1. Introduction

Terrestrial planets transmit heat from their interiors to their surfaces primarily via convection in the mantle (and sometimes the core) and then conduction through their solid lithospheres. This internal heat is a product of both the initial energy of planet formation, and of radioactive decay of long–lived radioisotopes, and can drive tectonic and volcanic activity as well as planetary magnetic dynamos. Measurements of heat flow through the upper layers of the crust can therefore help to constrain models of a particular planet's formation and composition, in addition to improving our understanding of its lithospheric thickness and crustal geology.

In the case of Mars, various compositional and heat transfer models predict a planetary heat flow of around $20 - 30$ mW m$^{-2}$ (Spohn et al., 2018, and references therein), or just under $20$ mW m$^{-2}$ (Ruiz et al., 2011; Parro et al., 2017; Egea-Gonzalez et al., 2017), with variations on this number able to differentiate between certain models (Plesa et al., 2015). The main goal of the $HP^3$ instrument on the InSight mission is therefore to measure this value for a representative site on Mars, by the use of a self–burrowing probe to record regolith temperatures up to 5 m into the subsurface. This should be deep enough to reach beyond the thermal waves induced by diurnal and annual temperature variations (Spohn et al., 2018), but may be still within the zone directly affected by longer term climate changes. These changes have previously been considered small compared to other perturbations on the global average heat flow, but may contribute a significant source of uncertainty to the $HP^3$ measurement that needs to be quantified.

The state of Mars' atmosphere and climate critically depends on the planet's obliquity and orbit (Laskar et al., 2004). It has been shown (Wood and Griffiths, 2007, 2009a,b, Wood et al., 2014) that changes in the planet's obliquity and orbit could trigger periodic collapse of the Martian atmosphere, which would lead to dramatic changes in regolith thermal conductivity and, therefore, subsurface heat transport.

During periods of low obliquity, occurring in cycles of roughly 120 kyr and 1.3 Myr periods, polar insolation is reduced, leading atmospheric $CO_2$ to condense onto the polar ice caps, thereby causing a dramatic reduction in surface pressure (Manning et al., 2006). Since the thermal conductivity of Martian dry regolith is dominated by gas filling the pore

spaces (Presley and Christensen, 1997), this leads to a corresponding decrease in its ability to transfer heat, resulting in a steeper temperature gradient in the regolith, and thus raising temperatures below the affected regolith layer. As atmospheric pressure, and regolith thermal conductivity, increases again, the heat stored underneath this insulating layer will diffuse away and the thermal gradient will return to its long–term equilibrium state. During this time, however, an increased heat flow (relative to average conditions) will be found in the near–surface, which may bias the results of the HP$^3$ experiment.

In this work, we therefore seek to model the propagation and decay of a subsurface heat accumulation caused by a temporary decrease in near–surface thermal conductivity, following the atmospheric pressure trends described in the literature. We then quantify the effects of the heat release on the present–day thermal profile, and discuss its potential detectability in (and/or biasing of) the results of a heat–flow experiment such as InSight's HP$^3$. Since the effect is small, we seek to place upper limits on its perturbation of present–day heat flow, i.e. the largest possible uncertainty on the InSight results due to this effect. The rest of the paper is outlined as follows. In Section 2, we describe in more detail the mechanism of atmospheric collapse and regolith thermal conductivity change, and examine estimates of its magnitude from the literature. In Section 3, we describe a simple numerical model developed to calculate the expected heat–flow perturbation from a given thermal conductivity change. In Section 4, we show the results of the model, validating it against the literature from Section 2, and examining the effects of varying key parameters. This is followed by a discussion, with references to the detectability by a heat–flow probe such as InSight, in Section 5, and our conclusions, in Section 6.

## 2. Background

### 2.1. Climate changes associated with obliquity cycles

The decrease in pressure during atmospheric collapse is found to be controlled by the thermodynamic balance between condensation and sublimation of $CO_2$ ice at the poles, which is, in turn, dependent on the ice's albedo (Manning et al., 2006; Wood and Griffiths, 2009a). Higher albedos mean more solar energy is reflected, reducing energy input and allowing more $CO_2$ to condense, increasing the magnitude of atmospheric collapse. This can be seen in Fig. 1, which shows atmospheric pressure over the last million years for several different polar albedos ($A_f$), as calculated by Manning et al. (2006) and Wood and Griffiths

(2009a). Periodic collapses following the 120 kyr obliquity cycle are visible, with a magnitude that is controlled by $A_f$ and ranges from the present–day ~650 Pa atmospheric pressure to a minimum of ~30 Pa. Some polar albedo values ($A_f \geq 0.7$) are effectively ruled out as they cannot reproduce present day pressures, while others ($A_f \leq 0.6$) do not produce any collapse in the last few hundred thousand years. Most models show a collapse to ~300 Pa around 40–50 kyr ago as the most recent.

In addition to atmospheric pressure changes, varying obliquity will also change average surface temperatures. Forget et al. (2013) show that global mean temperature is inversely correlated with obliquity, but that feedback effects (such as growth and retreat of the polar caps, with their above mentioned high albedo) mean the variation is small ($\lesssim 5$ K) between obliquities of ~$15 - 35°$, as occurred over the past Myr (Laskar et al., 2004). Local surface temperatures can vary significantly more than the global average of course, but Haberle et al. (2003) again show a relatively small ~$\pm 2$ K variation in equatorial annual mean surface temperature over this obliquity range.

### 2.2. Regolith response to changes in atmospheric pressure

$CO_2$ gas filling the regolith pores will respond quickly compared to the changing surface pressure curves of Fig. 1. Lorenz (2015), for example, calculate, based on experimentally measured diffusion co-efficients, that seasonal ~200 Pa pressure changes can propagate down to several hundred metres regolith depth within a single Martian year. Experimental work by Presley and Christensen (1997) has then found that regolith thermal conductivity $k$ is dominated by heat transport by the pore gas, and to empirically show a roughly power–law dependence on pressure (with an exponent of 0.6). Wood and Griffiths (2007) extended this with a more complicated first–principles model based on various parameters of porous materials (e.g. pore size, packing fraction and material bulk thermal conductivity). The behaviour of both models is similar for relevant Martian pressures, as shown by Wood and Griffiths (2007). Wood and Griffiths (2009b) list conductivities for fine-grained (100 μm particle diameter) and coarse-grained sand (500 μm particle diameter) as well as breccia (with a 1 cm grain size) at 600 and 30 Pa atmospheric pressures. Fig. 2 shows these values, alongside conductivities calculated at the same particle sizes with Eqn. (1) of Presley and Christensen (1997). Present–day regolith conductivities fall within the range given by Grott et al. (2007) and Morgan et al. (2017) for the material at the InSight landing site. Regolith conductivities during a severe
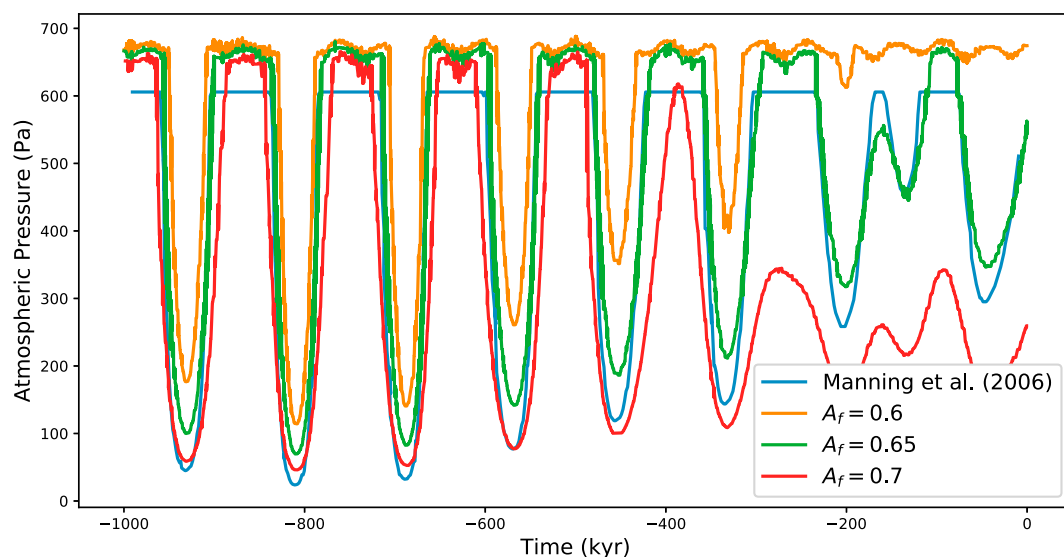


**Fig. 1.** Martian atmospheric pressure over the last million years, from climate models by Manning et al. (2006) and Wood and Griffiths (2009a) (for three different values of polar $CO_2$ ice albedo, $A_f$).
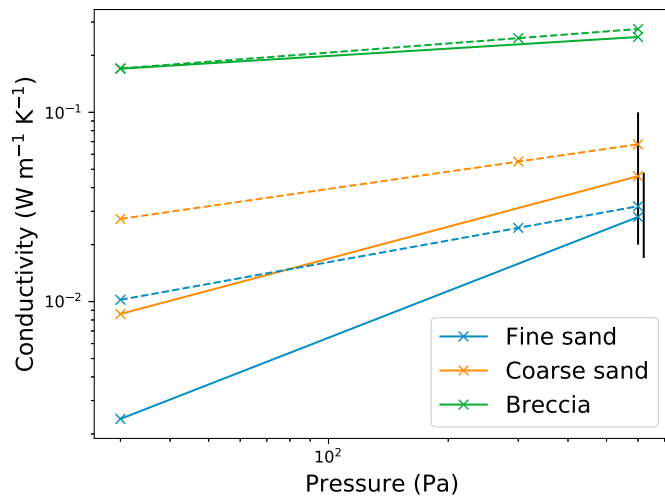
**Fig. 2.** Pressure dependence of thermal conductivity from Wood and Griffiths (2009b) (solid lines) and Presley and Christensen (1997) (dashed) for three different materials: fine sand of $100\,\mu m$ particle diameter, coarse sand of $500\,\mu m$, and breccia of $1\,cm$ size. Wood and Griffiths (2009b) values are taken from their Table 1 for $30\,Pa$ and $600\,Pa$ pressure, Presley and Christensen (1997) values are calculated for 30, 300 and $600\,Pa$ from their Eqn. (1). Vertical bars show the present–day thermal conductivity range expected for surface material at the InSight landing site from Grott et al. (2007) and Morgan et al. (2017) (offset for clarity).

atmospheric collapse are around five times smaller than present–day values for coarse sand and ten times smaller for fine sand.

### 2.3. Resulting heat–flow perturbation

Wood and Griffiths (2009b, a) coupled their regolith model with a climate model, using the time–varying atmospheric pressure of Manning et al. (2006) (blue curve in Fig. 1) to explore subsurface temperature changes over the last Myr of Martian history at a range of latitude locations and subsurface profiles (such as, typically $100\,m$ of fine or coarse-grained sand overlaying breccia and then solid rock).

In all cases, they found temperatures perturbed from the pre-collapse average, with a maximum perturbation occurring at the regolith/breccia boundary at depth $z_0$, explained by the thermal conductivity mismatch here when the regolith's thermal conductivity is drastically reduced, and the breccia's only slightly, during atmospheric collapse. Thus, the amount of geothermal heat escaping through the regolith is reduced and energy is stored below this more insulating layer, increasing temperatures. Over time, the temperature below the regolith keeps increasing until a new equilibrium state is reached that reflects the changed ratio of thermal conductivities above and below this boundary. However, long before this equilibrium can be reached, the atmospheric pressure is restored (essentially instantaneously, compared to the temperature response), regolith thermal conductivity increases again, and the subsurface temperature profile begins to return to the old, flatter profile. The increased temperature centred on $z_0$ diffuses and an increased heat flow is found until the background thermal balance is restored.

The temperature perturbation, relative to the background temperature structure, is a function of depth and time since the end of collapse, $\Delta T(z, t)$. Wood and Griffiths (2009b) show $\Delta T(z, t)$ for a number of different models and times, noting that the perturbation is largest (around $30\,K$ at the regolith/breccia boundary) just after the end of a collapse, and decays away towards the present day, while its magnitude is largely independent of latitude (and, therefore, of surface temperature trends). Typically the perturbation is only a few K at the present day.

We can calculate the transient excess heat flow associated with this perturbation by Grott et al. (2007):

$$\Delta F(z, t) = k \frac{\partial}{\partial z} \Delta T(z, t), \tag{1}$$

where $k$ is the present–day material thermal conductivity (since we are interested in the period after it has 'reset' to present–day atmospheric pressure values). Taking some examples from Wood and Griffiths (2009b), present–day gradients of around $0.02 - 0.03\,K\,m^{-1}$ are seen in the perturbation heat flow at $10°$ north latitude in the near surface for both coarse and fine-grained sand (i.e. $\Delta T(z_{0-5m}, t_{now})\tilde{~}0.02 - 0.03\,K\,m^{-1}$). Using Eqn. (1) with a present–day regolith thermal conductivity of $k = 0.02 - 0.1\,W\,m^{-1}\,K^{-1}$, as given by Grott et al. (2007), corresponds to perturbations of $0.4 - 3.0\,mW\,m^{-1}$, i.e. less than 10% of the assumed $30\,mW\,m^{-2}$ average geothermal heat flux.

In this study we aim to investigate the effect of such a temperature excursion on present–day heat-flow measurements such as InSight's HP[3]. According to Spohn et al. (2018) and Grott et al. (2019), the accuracy of the HP[3] instrument, when taking into account the known sources of uncertainty, should be $5 - 15\%$. Perturbations associated with atmospheric collapse would therefore be around the level of the existing noise, and their detection would appear challenging. Nevertheless, they may be have an important influence on the InSight results and might otherwise bias the final derived geothermal flux value, if their effects are not taken into account. We thus wish to investigate atmospheric collapse in more detail, noting that the work of Wood and Griffiths (2009b) was for a latitudinal location and regolith depth different to that of InSight's landing location. Below, we present a simple numerical model of the propagation of a thermal wave, associated with near–surface thermal conductivity changes, and examine the effects of various parameters on its perturbation to present–day heat flow. We consider this separately from the direct effects of the climate change itself, in order to quantify a strongest–case scenario for atmospheric collapse, to examine its detectability and whether it warrants detailed study with respect to InSight.

### 3. Method

We use a fully implicit, finite control volume approach (see, e.g. Patankar, 1980) to solve the one dimensional, time-dependent heat diffusion equation

$$\rho(z)c(z)\frac{\partial T}{\partial t} = \frac{\partial}{\partial z}\left(k(z)\frac{\partial T}{\partial z}\right). \tag{2}$$

Here $\rho$ and $c$ are the bulk density and specific heat, respectively, and temperature $T = T(z, t)$ is a function of both time and depth.

We define a simple three-layer structure, to represent regolith with a depth of $z_0$ with breccia/megaregolith below and bedrock below that. Regolith depth is expected to vary across the surface of Mars. In order for our results to be applicable to InSight, we need to take into account that unconsolidated surface material is thought to extend only $3 - 17\,m$ deep (Warner et al., 2017; Golombek et al., 2017) at the landing site, and so we investigate the effects of varying $z_0$ between 5 and $10\,m$, with a fixed $10\,m$ thick breccia layer between this and the bedrock, which itself extends to $2\,km$ depth.

Within each layer, the thermal conductivity is fixed at a single value, and the density and specific heat for both the regolith and breccia are set to $\rho = 1750\,kg\,m^{-3}$ and $c = 600\,J\,kg^{-1}\,K^{-1}$, respectively, as in Grott et al. (2007). Following Paton et al. (2016), the bedrock is set to $\rho = 2600\,kg\,m^{-3}$ and $c = 800\,J\,kg^{-1}\,K^{-1}$. In reality, thermal conductivity should be a function of time and depth, $k = k(z, t)$, dependent not just on the layering, but variations within the layers. Thermal conductivity in the near-surface regolith layer should increase with depth (due to decreasing porosity and/or a low $k$ surface dust layer), but, according to standard models (e.g. Grott et al., 2007), quickly approaches a constant value. Thus, below a few metres depth and within the regolith layer, thermal conductivity should be approximately constant, and a model with a constant value is therefore a reasonable approximation at the depths ($\geq 5$

m) and latitude (near equatorial, where ground ice is negligible) of interest to InSight. As noted above, the temperature perturbation effect comes from the difference between conductivities at layer boundaries, so by having sharp changes, rather than smoothly varying thermal conductivity with depth, we ensure that our model produces a maximum, strongest–case effect.

Since many of the parameters in Wood and Griffiths's model are largely unknown (e.g. polar albedo, regolith particle size, packing fraction and pore size, etc.), and we are interested in finding the maximum, worst-case scenario for the effects of atmospheric collapse, we follow several further approximations.

Firstly, we take a constant surface temperature (equal to the present–day seasonal average of 220 K at 4°N) as the top boundary condition (the bottom boundary condition is taken as a constant geothermal heat flux, $F = 20$ mW m$^{-2}$, as in Grott et al., 2007). A constant surface temperature is used, rather than a time-varying climate model, to investigate purely the effects of thermal conductivity changes as distinct from the direct temperature changes associated with the obliquity cycles. This is justified by the small variations in mean annual surface temperature, as noted in section 2.1, as well as the swift decay with time of their effects, as noted by Grott et al., and the minimal effect on subsurface perturbations the surface temperature is noted to have by Wood and Griffiths.

Secondly, we simplify the collapse itself to avoid the complication of the many unknown parameters. We set the thermal conductivities to those appropriate for some pressure P, followed by a return to present–day values after a set duration (essentially taking a square well pressure–time dependence, rather than choosing one of the curves of Fig. 1). This means we get the maximum possible temperature increase at $z_0$, as thermal conductivity is always at its minimum during the entire duration of the collapse.

The procedure is as follows: the model is run for several thousand years with present–day thermal conductivities, to reach an equilibrium temperature profile. Conductivities are decreased to their atmospheric collapse values for some duration and then returned to their present values. The perturbed temperature profile, relative to the pre–collapse equilibrium, is measured immediately after the end of the collapse and for up to 1 Myr subsequently, in order to observe its decay towards the background temperature profile. We vary the duration of the collapse, as well as the depth of the regolith/breccia boundary, their conductivities, and the minimum atmospheric pressure, to investigate their effects on the subsurface temperature.

## 4. Results

We first validate our model by reproducing the results of Wood and Griffiths (2009b). Using a $z_0 = 100$ m deep regolith layer of coarse sand over breccia and rock (conductivities of $k = 0.046, 0.25$ and $2$ W m$^{-1}$ K$^{-1}$, respectively) and a 30 kyr collapse to 30 Pa (collapse conductivities of $k = 0.0086, 0.17$ and $2$ W m$^{-1}$ K$^{-1}$, respectively), we find a maximum ~30 K temperature perturbation at $z_0$, that decays to a few K at present day, matching the results of Wood and Griffiths (2009b).

Next, we consider the effect of the heat–flow perturbation on the InSight measurements by selecting a subsurface structure more appropriate for the InSight landing site. Fig. 3 (first row) shows the temperature perturbation, $\Delta T(z, t)$, at the end of collapse for three different collapse durations, and regolith depths of 5 and 10 m of coarse sand. Thinning the insulating regolith layer reduces the proportion of geothermal heat retained below, resulting in much smaller temperature perturbations than given by Wood and Griffiths (2009b). The maximum perturbation is now around 10 K.

When we now advance our simple thermal model forwards in time, after the end of the atmospheric collapse, the heat pulse is observed to decay back to background conditions. At each time and depth we can calculate the excess heat flow which would be seen, above the average geothermal flux, by subtracting the background profile away to find $\Delta T(z, t)$, and then using Eqn. (1), with present–day conductivities. Fig. 4
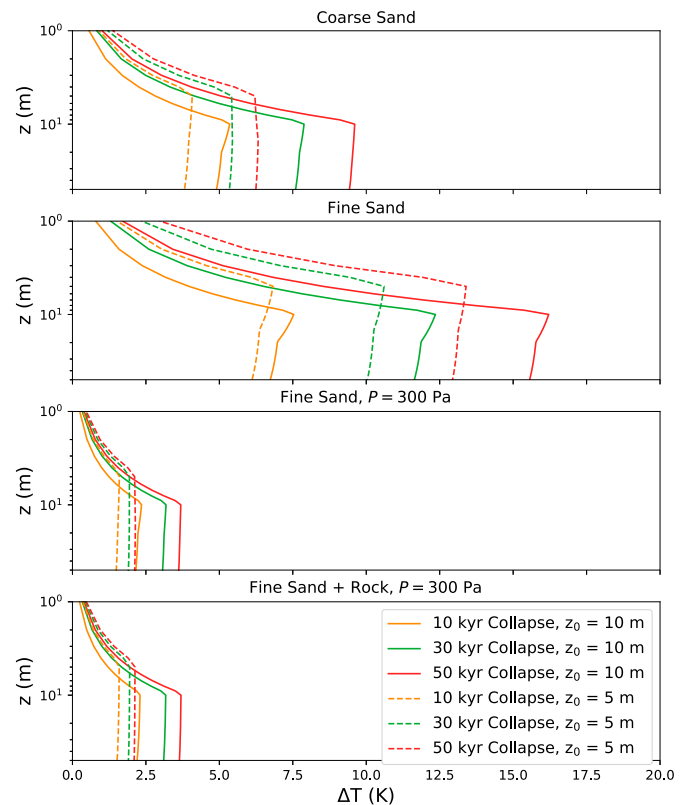


**Fig. 3.** Temperature perturbations expected at the end of an atmospheric collapse from various periods of reduced regolith thermal conductivity with varying regolith depth $z_0$ (solid: $z_0 = 10$ m, dashed: $z_0 = 5$ m). The scenarios are, from top: collapse to 30 Pa with coarse–grained regolith, collapse to 30 Pa with fine–grained regolith, collapse to 300 Pa with fine–grained regolith, and collapse to 300 Pa with fine–grained regolith overlaying bedrock.

(first row) shows the heat–flow perturbation with time since the end of the collapse, at the InSight measurement depth ($z = 5$ m), for each of the regolith depths and collapse durations from above. In all cases the initially large perturbation is negligible after a few hundred thousand years. The nominal $z_0 = 10$ m, 30 kyr perturbation decays away to around 15% of the assumed 20 mW m$^{-2}$ heat flux after ~40 kyr, while the effect is larger/smaller for longer/shorter collapse durations and thicker/thinner regolith.

As discussed above, the temperature perturbation arises at the boundary between two layers of differing conductivities, so what happens if this difference is greater? We replace the coarse sand conductivities with the smaller values for fine sand from Wood and Griffiths (2009b) ($k = 0.028$ and $0.0024$ W m$^{-1}$ K$^{-1}$ for 600 and 30 Pa, respectively), keeping the breccia and bedrock the same, and repeat the experiment. The second rows of Figs. 3 and 4 show the resulting temperature and heat–flow perturbations, respectively. Sure enough, the smaller regolith conductivities, relative to the unchanged breccia values, means that the fine sand acts as a better insulator, trapping more geothermal heat during collapse. Upon return to present pressures, the large temperature perturbation takes longer to diffuse away, leading to increased heat–flow perturbations, i.e. over 20% of present–day heat flow for the 30 kyr case after 40 kyr, and nearly 40% for a 50 kyr collapse!

The above would be significant perturbations and should be detectable by HP[3] on InSight. However, noting Fig. 1, the chance of a recent collapse reaching 30 Pa atmospheric pressures appear very remote. The models suggest that recent collapses, in the last few hundred thousand years, only reach a minimum pressure of around 300 Pa. We therefore investigate such a collapse by using the present–day thermal conductivity of fine sand from Wood and Griffiths (2009b), and interpolating a value
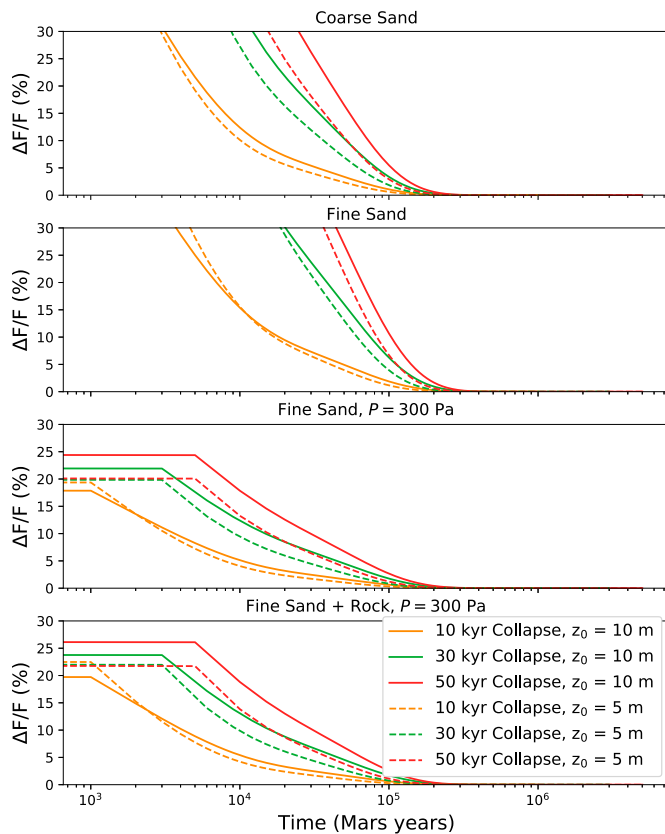
**Fig. 4.** Heat–flow perturbations, with time since the end of an atmospheric collapse, expected at 5 m depth (solid: $z_0 = 10$ m, dashed: $z_0 = 5$ m). The scenarios are, from top: collapse to 30 Pa with coarse–grained regolith, collapse to 30 Pa with fine–grained regolith, collapse to 300 Pa with fine–grained regolith, and collapse to 300 Pa with fine–grained regolith overlaying bedrock.

at 300 Pa pressure from the log–log plot (Fig. 2) of $k = 0.016$ W m$^{-1}$ K$^{-1}$. We do this, rather than using the Presley and Christensen (1997) results shown in the same plot, both for consistency with our previous models, and because, as can be seen in the plot, the Wood and Griffiths (2009b) conductivities decay fastest with pressure, again giving us a strongest–case effect.

Row three of Figs. 3 and 4 show the resulting temperature and heat–flow perturbations. As expected, temperature perturbations are now much reduced, not exceeding 5 K in any of the models. This results in smaller heat–flow perturbations of between ~2 − 8% and around 5.5% for a 30 kyr collapse and 10 m of regolith. Perturbations will be even smaller for coarser grained material.

Finally, we can ask what the perturbations would look like in a situation where the fine-grained regolith layer overlays solid bedrock directly, with no intermediate breccia/megaregolith layer. The large thermal conductivity mismatch at $z_0$ might be expected to produce a large temperature perturbation here, but as shown in the bottom row of Figs. 3 and 4, the effects are similar to the above three-layered cases, with an only slightly larger perturbation. This demonstrates that it is the properties of the regolith (i.e. its thickness, present–day thermal conductivity and corresponding pressure dependence), and the collapse itself (duration and minimum pressure reached), that are the dominant factors in determining the heat–flow perturbation associated with atmospheric collapse.

## 5. Discussion

We have presented upper limits for the ability of thermal conductivity changes due to atmospheric collapse to perturb present–day heat flow on

Mars. In particular, these are upper limits because regolith thermal conductivity should decrease near the surface, reducing heat–flow perturbations here. Although our model of an instantaneous change in thermal conductivity is relatively simple, the conclusions drawn from it are relatively robust. Thermal conductivity changes which smoothly follow the pressure curves of Fig. 1, rather than changing instantaneously as in our model, would lead to a regolith that spends less time as an effective insulating layer, reducing heat build up. Additionally, smoothly varying regolith size/thermal conductivity with depth would also reduce the thermal conductivity difference at the layer boundaries, again resulting in smaller perturbations than presented here.

We thus conclude that our estimated heat–flow perturbation, of around ~2 − 8% for an atmospheric collapse to 300 Pa in the last 40 kyr, is a reasonable upper limit. Coarser grained material, towards the higher end of the expected thermal conductivity range, would lead to even smaller perturbations. This is the positive excess we would expect a present–day heat–flow experiment such as InSight's HP[3] to measure, on–top of an average geothermal flux of $F = 20$ mW m$^{-2}$. If a severe atmospheric collapse to 30 Pa occurred around 40 kyr ago, the perturbations could be larger, up to ~20 − 40%, but this is considered unlikely (Manning et al., 2006; Wood and Griffiths, 2007). In relation to the InSight measurements, it is instructive to compare this heat–flow perturbation to those estimated for other sources of uncertainty considered.

Spohn et al. (2018) break down the error budget from sources relating to the HP[3] measurement process itself, as well as the external uncertainty which comes from averaging out the annual thermal wave. They estimate a total uncertainty of 2.2 mW m$^{-2}$ or 10.8% for the nominal case of the instrument reaching 3 m depth. If the probe reaches the full 5 m depth, the 10% of this error coming from of the annual heatwave is reduced and Spohn et al. estimate a 5% uncertainty. Both these estimates are for 0.6 Martian years worth of measurements. If the full year's worth can be obtained, the annual heatwave error can be even further reduced, but the total instrument error of around 4% is unlikely to be improved upon. Thus, in the relatively optimistic scenario of good instrument deployment and full measurement time, our maximum-strength atmospheric collapse signal may just be detected above the error bars; whereas, in the worst-case scenario, it is likely to be lost in the instrument noise.

Further sources of error are not taken into account by Spohn et al.. For example, Grott et al. (2007) estimate the perturbation caused by the direct surface temperature changes due to the obliquity cycles themselves. Modelling the propagation of thermal waves into an homogeneous semi-infinite half space, they estimate perturbations of a few percent, for a 10 K step-change $0.1 − 1$ Myr before present, and by $< 15\%$, for 10 K periodic forcing every 120 kyr. From the discussion in Section 2 above, this appears to be too large. Assuming instead periodic forcing with an amplitude of $\pm 2$ K in surface temperature, we can use Grott et al.'s Eqn. 6 with $k = 0.046$ W m$^{-1}$ K$^{-1}$ to estimate a present-day perturbation of ~1.5% at 5 m depth. The direct temperature perturbation of the obliquity cycles therefore appears to be similar to, or smaller than, the thermal conductivity change effect, for reasonable parameter choices.

Additionally, if the recent (centuries before present) Little Ice Age on Earth was caused by solar changes and also affected Mars, it might cause perturbations of $5 − 10\%$, according to Lorenz (2015). Morgan et al. (2017), meanwhile, showed that atmospheric convection into the HP[3] borehole should be negligible, but that changes in surface temperature from dust redistribution during landing may have an effect. After landing, shadowing by and re–radiation from the lander will also cause temperature changes to propagate into the subsurface. According to thermal modelling by Siegler et al. (2017), these should be limited to $\Delta F < 3$ mW m$^{-2}$, or 15%, when measured below 1 m and away from lander body, although complicated seasonal changes may need to be averaged out over time. Finally, local dust storms reduce atmospheric opacity and redistribute surface dust, and can perturb heat flow by 2 mW m$^{-2}$ to depths of up to $1 − 2$ m (for $k = 0.02 − 0.05$ W m$^{-1}$ K$^{-1}$),

while global dust storms, as occurred in Mars year 28, can cause $1.5 - 2.5$ mW m$^{-2}$ perturbations as deep as $2 - 3$ m (Plesa et al., 2016).

All of these additional perturbations are of a similar magnitude to those expected from thermal conductivity changes associated with atmospheric collapse. We note, however, that the presence of a dust storm is easily observed and it should, therefore, be possible to model its effect and recover a good estimate of the undisturbed geothermal flux. This is similarly the case for the lander, re-radiation and shadowing, which can be modelled as shown by Siegler et al. (2017). Assuming good instrument deployment, full spacecraft functionally over a Martian year and a well–modelled surface configuration, the largest perturbations are therefore those associated with climate change, e.g. several percent flux change from the direct effect of the obliquity cycles, $\sim 2 - 8\%$ change from atmospheric collapse associated with them, and $5 - 10\%$ from any recent Little Ice Age.

Disentangling these different climate change signals from their magnitudes alone will be difficult. Can we say anything more about the direction of the signals, or how they vary in time and depth? Fig. 5 shows the depth profile of the atmospheric collapse heat-flow perturbation at 40 kyr after the end of our nominal 30 kyr collapse (for the strongest-case scenario of fine-grained regolith and a collapse to 30 Pa). The gradient of the perturbation (the 'gradient of the gradient' of the temperature) is essentially constant until several hundred metres depth, precluding any measurement of it by InSight. Can any information be gained from the decay with time of a historical heat pulse? We found that the change in heat flow over one simulation time–step (roughly 3000 years) is $\sim 1\%$, so only a small fraction of a percent per year. Considering InSight's nominal mission length, this is far below the ability of HP$^3$ to detect. Lorenz (2015) likewise showed that the Little Ice Age signature would not show any gradient at the depths to be probed by InSight.

Mean surface temperature is inversely correlated with obliquity (Haberle et al., 2003; Forget et al., 2013), so the most recent phase of low obliquity, 40 kyr ago, will have led to a small positive excess heatwave, in the same direction as our atmospheric collapse signal. On the other hand, the Little Ice Age would have induced a small negative temperature perturbation. Thus, the two effects might cancel each-other out; or, a suspicious, otherwise unaccounted-for bias in the InSight results, in one direction or the other, might hint at which past climate effect dominates.

If we cannot definitively distinguish the climate change effects, then they will have to be treated as another source of uncertainty, to be mixed in with the instrument error. The total uncertainty would then be $\sim \sqrt{4\%^2 + 5\%^2 + 5\%^2} \sim 8\%$ (for Little Ice Age and atmospheric collapse

signals of 5%), which would set the minimum HP$^3$ error level and could not be improved upon with deeper or longer measurements.

## 6. Conclusion

We estimated the effects on the present–day Martian heat flow of regolith thermal conductivity changes associated with past periods of putative atmospheric collapse, and put them into the context of the InSight heat–flow experiment HP$^3$. During these periods, obliquity changes lead atmospheric $CO_2$ to condense out onto the Martian poles, drastically lowering atmospheric pressure and reducing regolith thermal conductivity. Changes in the subsurface temperature profile, as it adjusts to varying thermal conductivity, can then persist for tens of thousands of years and perturb the present–day apparent heat flow.

We used a simple numerical model to calculate the build-up and diffusion of a heat pulse from a recent (40 kyr ago) atmospheric collapse, varying the duration and severity of the collapse, and the depth of the regolith layer to quantify their effects. For $5 - 10$ m thick regolith layers and the most likely collapse severity, we find subsurface temperatures perturbed by less than 10 K at the end of the collapse which, when evolved forwards with time, corresponds to perturbations of $\sim 2 - 8\%$ of present–day heat flow. This is the positive excess we would expect to measure, on–top of an average geothermal flux of $F = 20$ mW m$^{-2}$.

InSight should measure Martian heat flow to an accuracy of between 5 and 15% (with an instrumental limit of around 4%) with its HP$^3$ instrument. Thus, in the strongest–case scenario (of full instrument deployment, a complete measurement campaign, and a well-modelled surface configuration), the effects of past atmospheric collapse may be encountered as a slight increase of a few percent in present–day heat flow. Nonetheless, distinguishing this increase from a higher than expected average flux, as well as other climactic changes such as a Little Ice Age, will be challenging, unless a heat–flow measurement can accurately monitor subsurface temperatures for several 100 years and/or measure several 100 m below the surface. As also noted by Lorenz (2015), the full characterisation of long time-scale perturbations to subsurface temperature requires extremely deep measurements, to depths similar to their skin depths of tens to hundreds of metres, which remains out of the scope of current or near future space missions.

Thus, past climate changes will only be significant as a relatively minor source of added uncertainty in the HP$^3$ measurement. If InSight's measurement accuracy proves better than expected (and the other sources of error, such as surface albedo changes, shadowing and re-radiation from the lander, are well understood) then a more detailed model of past climate, incorporating surface temperature trends and gradual rather than instantaneous changes in thermal conductivity, and using in situ determined conductivity, could be considered to further constrain the estimated heat flow perturbation.

**Fig. 5.** Heat-flow perturbation with depth for two times after the end of an extreme atmospheric collapse to 30 Pa, and regolith depths $z_0 = 10$ m (solid) and $z_0 = 5$ m (dashed). Gradients in the region of interest are essentially constant, and changes with time negligible for this timeframe.

## References

Egea-Gonzalez, I., Jiménez-Díaz, A., Parro, L.M., López, V., Williams, J.P., Ruiz, J., 2017. Thrust fault modeling and Late-Noachian lithospheric structure of the circum-Hellas region, Mars. Icarus 288, 53–68. https://doi.org/10.1016/j.icarus.2017.01.028.

Forget, F., Wordsworth, R., Millour, E., Madeleine, J.B., Kerber, L., Leconte, J., Marcq, E., Haberle, R., 2013. 3d modelling of the early martian climate under a denser co2 atmosphere: temperatures and co2 ice clouds. Icarus 222, 81–99. https://doi.org/10.1016/j.icarus.2012.10.019. http://www.sciencedirect.com/science/article/pii/S0019103512004265.

Golombek, M., Kipp, D., Warner, N., Daubar, I.J., Fergason, R., Kirk, R.L., Beyer, R., Huertas, A., Piqueux, S., Putzig, N.E., Campbell, B.A., Morgan, G.A., Charalambous, C., Pike, W.T., Gwinner, K., Calef, F., Kass, D., Mischna, M., Ashley, J., Bloom, C., Wigton, N., Hare, T., Schwartz, C., Gengl, H., Redmond, L., Trautman, M., Sweeney, J., Grima, C., Smith, I.B., Sklyanskiy, E., Lisano, M., Benardini, J.,
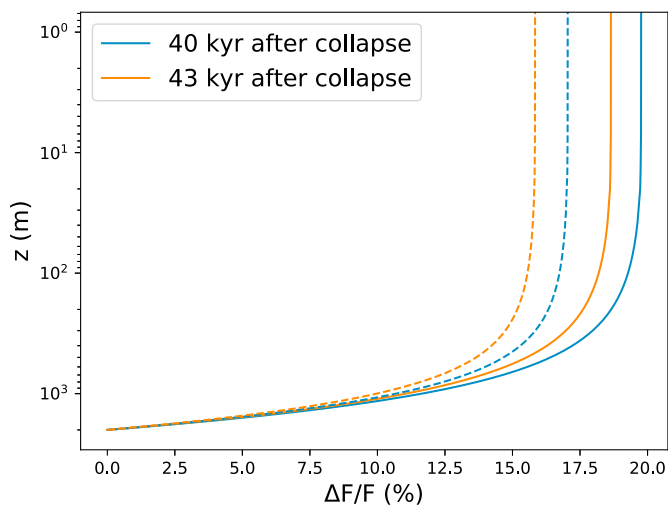
Smrekar, S., Lognonné, P., Banerdt, W.B., 2017. Selection of the InSight landing site. Space Sci. Rev. 211, 5–95. https://doi.org/10.1007/s11214-016-0321-9.

Grott, M., Helbert, J., Nadalini, R., 2007. Thermal structure of Martian soil and the measurability of the planetary heat flow. J. Geophys. Res. 112, E09004. https://doi.org/10.1029/2007JE002905.

Grott, M., Spohn, T., Knollenberg, J., Krause, C., Scharringhausen, M., Wippermann, T., Smrekar, S., Hudson, T., Banerdt, w., 2019. Calibration of the heat flow and physical properties package (hp3) for the insight mars mission. Earth and Space Sci. (in revision).

Haberle, R.M., Murphy, J.R., Schaeffer, J., 2003. Orbital change experiments with a mars general circulation model. Icarus 161, 66–89. https://doi.org/10.1016/S0019-1035(02)00017-9. http://www.sciencedirect.com/science/article/pii/S0019103502000179.

Laskar, J., Correia, A.C.M., Gastineau, M., Joutel, F., Levrard, B., Robutel, P., 2004. Long term evolution and chaotic diffusion of the insolation quantities of Mars. Icarus 170, 343–364. https://doi.org/10.1016/j.icarus.2004.04.005.

Lorenz, R.D., 2015. Meteorological insights from planetary heat flow measurements. Icarus 250, 262–267. https://doi.org/10.1016/j.icarus.2014.11.021.

Manning, C.V., McKay, C.P., Zahnle, K.J., 2006. Thick and thin models of the evolution of carbon dioxide on mars. Icarus 180, 38–59. https://doi.org/10.1016/j.icarus.2005.08.014. http://www.sciencedirect.com/science/article/pii/S0019103505003209.

Morgan, P., Smrekar, S.E., Lorenz, R., Grott, M., Kroemer, O., Müller, N., 2017. Potential effects of surface temperature variations and disturbances and thermal convection on the mars InSight HP$^3$ heat-flow determination. Space Sci. Rev. 211, 277–313. https://doi.org/10.1007/s11214-017-0388-y.

Parro, L.M., Jiménez-Díaz, A., Mansilla, F., Ruiz, J., 2017. Present-day heat flow model of Mars. Sci. Rep. 7, 45629. https://doi.org/10.1038/srep45629.

Patankar, S.V., 1980. Numerical Heat Transfer and Fluid Flow. Hemisphere Publishing Corp., Washington, DC, p. 210, 1980.

Paton, A.M., Harri, A.M., Savijärvi, H., Mäkinen, T., Hagermann, A., Kemppinen, O., Johnston, A., 2016. Thermal and microstructural properties of fine-grained material at the Viking Lander 1 site. Icarus 271, 360–374. https://doi.org/10.1016/j.icarus.2016.02.012.

Plesa, A.C., Grott, M., Lemmon, M.T., Müller, N., Piqueux, S., Siegler, M.A., Smrekar, S.E., Spohn, T., 2016. Interannual perturbations of the Martian surface heat flow by atmospheric dust opacity variations. J. Geophys. Res. 121, 2166–2175. https://doi.org/10.1002/2016JE005127.

Plesa, A.C., Tosi, N., Grott, M., Breuer, D., 2015. Thermal evolution and urey ratio of mars. J. Geophys. Res.: Planets 120, 995–1010. https://doi.org/10.1002/2014JE004748.

Presley, M.A., Christensen, P.R., 1997. The effect of bulk density and particle size sorting on the thermal conductivity of particulate materials under Martian atmospheric pressures. J. Geophys. Res. 102, 9221–9230. https://doi.org/10.1029/97JE00271.

Ruiz, J., McGovern, P.J., Jiménez-Díaz, A., López, V., Williams, J.P., Hahn, B.C., Tejero, R., 2011. The thermal evolution of Mars as constrained by paleo-heat flows. Icarus 215, 508–517. https://doi.org/10.1016/j.icarus.2011.07.029.

Siegler, M.A., Smrekar, S.E., Grott, M., Piqueux, S., Mueller, N., Williams, J.P., Plesa, A.C., Spohn, T., 2017. The InSight mars lander and its effect on the subsurface thermal environment. Space Sci. Rev. 211, 259–275. https://doi.org/10.1007/s11214-017-0331-2.

Spohn, T., Grott, M., Smrekar, S.E., Knollenberg, J., Hudson, T.L., Krause, C., Müller, N., Jänchen, J., Börner, A., Wippermann, T., Krömer, O., Lichtenheldt, R., Wisniewski, L., Grygorczuk, J., Fittock, M., Rheershemius, S., Spröwitz, T., Kopp, E., Walter, I., Plesa, A.C., Breuer, D., Morgan, P., Banerdt, W.B., 2018. The heat flow and physical properties package (HP3) for the InSight mission. Space Sci. Rev. 214, 96. https://doi.org/10.1007/s11214-018-0531-4.

Warner, N.H., Golombek, M.P., Sweeney, J., Fergason, R., Kirk, R., Schwartz, C., 2017. Near surface stratigraphy and regolith production in Southwestern Elysium Planitia, mars: implications for Hesperian-Amazonian terrains and the InSight lander mission. Space Sci. Rev. 211, 147–190. https://doi.org/10.1007/s11214-017-0352-x.

Wood, S.E., Griffiths, S.D., 2007. Mars subsurface warming at low obliquity. Seventh Int. Conf. Mars 1353, 3387.

Wood, S.E., Griffiths, S.D., 2009a. Epochal seasonal thermal modeling of mars' polar surface energy balance: perennial CO2 ice and atmospheric collapse. In: Third International Workshop on Mars Polar Energy Balance and the CO2 Cycle, 1494, pp. 65–66.

Wood, S.E., Griffiths, S.D., 2009b. Mars subsurface warming due to atmospheric collapse at low obliquity. Lunar Planet. Sci. Conf. 40, 2490.

Wood, S.E., Griffiths, S.D., Bapst, J.N., 2014. Mars at low obliquity: perennial CO2 caps, atmospheric collapse, and subsurface warming. Eighth Int. Conf. Mars 1791, 1495.